Modeling and Scaling Coupled Energy, Water, and Carbon Fluxes Based on Remote Sensing: An Application to Canada's Landmass

BAOZHANG CHEN, JING M. CHEN, GANG MO, AND CHIU-WAI YUEN

Department of Geography and Program in Planning, University of Toronto, Toronto, Ontario, Canada

HANK MARGOLIS

Faculté de Foresterie et de Géomatique, Université Laval, Quebec City, Quebec, Canada

KAZ HIGUCHI AND DOUGLAS CHAN

Air Quality Research Branch, Meteorological Service of Canada, Toronto, Ontario, Canada

(Manuscript received 24 May 2005, in final form 4 August 2006)

ABSTRACT

Land surface models (LSMs) need to be coupled with atmospheric general circulation models (GCMs) to adequately simulate the exchanges of energy, water, and carbon between the atmosphere and terrestrial surfaces. The heterogeneity of the land surface and its interaction with temporally and spatially varying meteorological conditions result in nonlinear effects on fluxes of energy, water, and carbon, making it challenging to scale these fluxes accurately. The issue of up-scaling remains one of the critical unsolved problems in the parameterization of subgrid-scale fluxes in coupled LSM and GCM models.

A new distributed LSM, the Ecosystem–Atmosphere Simulation Scheme (EASS) was developed and coupled with the atmospheric Global Environmental Multiscale model (GEM) to simulate energy, water, and carbon fluxes over Canada's landmass through the use of remote sensing and ancillary data. Two approaches (lumped case and distributed case) for handling subgrid heterogeneity were used to evaluate the effect of land-cover heterogeneity on regional flux simulations based on remote sensing. Online runs for a week in August 2003 provided an opportunity to investigate model performance and spatial scaling issues.

Comparisons of simulated results with available tower observations (five sites) across an east–west transect over Canada's southern forest regions indicate that the model is reasonably successful in capturing both the spatial and temporal variations in carbon and energy fluxes, although there were still some biases in estimates of latent and sensible heat fluxes between the simulations and the tower observations. Moreover, the latent and sensible heat fluxes were found to be better modeled in the coupled EASS–GEM system than in the uncoupled GEM. There are marked spatial variations in simulated fluxes over Canada's landmass. These patterns of spatial variation closely follow vegetation-cover types as well as leaf area index, both of which are highly correlated with the underlying soil types, soil moisture conditions, and soil carbon pools. The surface fluxes modeled by the two up-scaling approaches (lumped and distributed cases) differ by 5%–15% on average and by up to 15%–25% in highly heterogeneous regions. This suggests that different ways of treating subgrid land surface heterogeneities could lead to noticeable biases in model output.

1. Introduction

The development of land surface models (LSMs) from early simple models to more recent detailed models that include carbon exchange has been reviewed by Pitman (2003). As illustrated by Chen et al. (2007, manuscript submitted to *Ecol. Modell.*, hereafter C07), the importance of LSMs has been increasingly recognized in modeling both surface microclimate and the large-scale atmosphere (e.g., Dickinson et al. 1986, 1992; Garratt 1993; Sellers et al. 1986, 1997a,b; Pitman 2003; Pleim and Xiu 2003). Significant problems related to LSMs, however, have yet to be addressed, including the difficulties in parameterizing hydrological processes, root processes, subgrid-scale heterogeneity, and biogeochemical cycles (Pitman 2003).

Corresponding author address: Dr. Baozhang Chen, Biometeorology and Soil Physics Group, Faculty of Land and Food Systems, University of British Columbia, 2357 Main Mall, Vancouver, BC V6T 1Z4, Canada.
E-mail: Baozhang.Chen@ubc.ca

DOI: 10.1175/JHM566.1

It has also been recognized that LSMs need to be coupled with atmospheric general circulation models (GCMs) to adequately simulate the surface fluxes of energy, water, and carbon (Sellers et al. 1996; Garratt 1993; Saunders et al. 1999). Depending on individual situations, LSMs are built with different emphases, complexities, input requirements, and temporal and spatial resolutions. Existing LSMs are usually validated at local scales (i.e., <1 km^2) using flux tower data (Kimball et al. 1999). GCMs and regional models, however, generally define land surface conditions and fluxes at larger scales (i.e., >100 km^2), where minimum grids (pixels) often represent area averages of highly heterogeneous surface features. An important question is how to best aggregate a finer resolution (microscale LSMs) to a coarser resolution and still be consistent with macroscale GCMs when the two models are coupled.

Current LSMs can be categorized into two groups regarding the treatment of land surface heterogeneity. One group is "aggregated models" with spatial characteristics of biospheric processes assumed to be homogeneous within a model's grid (pixel). This group includes the Biosphere–Atmosphere Transfer Scheme (BATS) (Dickinson et al. 1986), the Simple Biosphere Model version 2.0 (SiB2) (Sellers et al. 1996), and the Ecosystem–Atmosphere Simulation Scheme (EASS) (C07). Another group considers subgrid heterogeneity at varying levels of detail, from fractional areas to statistical distributions (Abramopoulos et al. 1988; Entekhabi and Eagleson 1989), for example, the Interactions between Soil–Biosphere–Atmosphere (ISBA) scheme (Bélair et al. 2003) and the Canadian Land Surface Scheme (CLASS) (Verseghy 1991; Verseghy et al. 1993).

LSMs often have to be simplified when coupled to GCMs because of the constraints caused by the availability of land surface data. However, this shortcoming was overcome in this study by incorporating remote-sensing-derived parameter maps of key state variables [land-cover type (LC), leaf area index (LAI), and clumping index (Ω)] at different spatial scales. These variables are used to determine energy and water partitioning and photosynthesis as described previously (Kite and Pietroniro 1996; Rango and Shalaby 1999; Liu et al. 2003). Because remotely sensed data have the advantage of large area coverage, frequent updating and consistent quality, satellite observations have been used to describe the phenology of vegetation as input data for land surface schemes (e.g. Sellers et al. 1996). Oleson and Bonan (2000) described and tested a method for incorporating remotely sensed subgrid-scale plant functional type and LAI data into a land surface scheme in a climate model and concluded that satellite-derived data were most useful for improving the description of spatial variability of the surface energy fluxes.

Spatial heterogeneity of the land surface introduces major uncertainties in large-scale analyses (Ehleringer and Field 1993). The complex heterogeneity of the land surface through vegetation, soils, topography, and their interaction with temporally and spatially varying meteorological variables results in nonlinear effects on fluxes of energy, water, and carbon. The issue of up-scaling is one of the critical unsolved problems for the parameterization of coupled LSM and GCM models (Wood and Lakshmi 1993).

Land-cover features essential for characterizing regional physical processes may not be able to be distinguished at coarse spatial resolutions (Kimball et al. 1999). Some land covers, even with low fractions, are essential for characterizing regional fluxes and may be omitted at coarse spatial resolutions. Wetlands, for example, represent less than 7% of the Boreal Ecosystem–Atmosphere Study (BOREAS) southern study area (SSA) but may play an important role in the regional carbon balance (Roulet et al. 1997). Needleleaf coniferous forests have also been found to be quite different from deciduous forest in net photosynthesis. Unfortunately, these characteristics may not be adequately represented at macroscales in GCMs. A key issue of up-scaling is the proper consideration of subgrid land-cover features on regional energy, water, and carbon fluxes.

The purposes of this study are threefold: (i) to test and verify the capability and accuracy of the EASS model when coupled to a GCM model and applied to a large area with significant heterogeneity, such as the Canada's landmass; (ii) to evaluate the effect of land-cover heterogeneity on regional energy, water, and carbon flux simulation based on remote sensing data; and (iii) to explore up-scaling methodologies using satellite-derived data. In this paper, we briefly present a basic theoretical examination of spatial up-scaling (section 2) and then outline the land surface and atmospheric model (section 3). A description of the dataset used for modeling follows in section 4. Model results for the Canadian landmass for the period of 13 to 19 August 2003 are discussed in section 5 and are followed by conclusions.

2. Theory and algorithms for spatial scaling

a. Theory

General scaling issues related to understanding ecosystem function and predicting the consequences of

global environment change were reviewed by Jarvis (1995). The scaling issues usually include defining the spatial and temporal scales of interest, scaling processes, scaling strategy, scaling problems, heterogeneity, patchiness, nonlinearity, aggregation methodology, and feedbacks. Scaling theories have provided important clues toward understanding and modeling the space–time dynamics of diverse biogeophysical processes (Poveda and Luis 2004), such as vegetation surface fluxes (Katul et al. 2001), ecological processes (Bascompte and Sole 1998; Tilman and Kareiva 1997), and vegetation dynamics (Harte et al. 1999; Milne and Cohen 1999; Milne et al. 2002).

In this paper, we focus on the issue of spatial upscaling related to model coupling. Land surface processes take place at spatial scales ranging from the size of small vegetation patches up to the extent of the globe itself (Jarvis 1995). Generally, the objective of upscaling is to preserve or to transport certain rate processes, such as flux densities, from smaller spatial scales to larger ones. This would be very easy to achieve if the produced fluxes or rates were linearly related to all static and driving variables. Unfortunately, in nature, this is not usually the case. What makes up-scaling such a significant challenge is the nonlinearity between processes and variables and the spatial heterogeneity in surface and atmospheric properties. As mentioned earlier, the EASS model is similar to most process models and represents point-level processes using functional relationship between input variables and output fluxes. However, it ignores or greatly simplifies the effects of spatial heterogeneity in the driving variables within the model's smallest grid. Biased results may be produced if the homogeneity assumption or the simple arithmetic average at local scales is applied to a complex surface at regional scales when coupled to GCMs because the characterization of regional fluxes are affected by both the influence of subgrid-scale processes within the aggregate and the degree of nonlinearity between the model inputs and outputs (Kimball et al. 1999). The propagation of errors among the various functional relationships in a GCM's framework may also be additive or compensatory depending on the particular process being simulated (Sellers et al. 1992; Rastetter et al. 1992; Band 1993; Pierce and Running 1995; Kimball et al. 1999).

The sensitivities of a land surface scheme and an ecological model to spatial scale have been found to vary depending on the surface conditions and input variables (Kimball et al. 1999). Among the variables, land-cover type was also found to be most important for flux simulations (Bonan 1993; Sellers et al. 1995). If a critical land-cover characteristic is inadequately presented for coarse-resolution grids within the large model framework, then significant biases may occur in the coupled-model simulations. The issue of how best to aggregate finescale data to a large scale is complex, and the optimal approach is to some degree unique to each variable. It has been found that contextural parameters are more efficient than textural parameters (Chen et al. 1999). A contextural approach of spatial scaling makes use of area fractions to derive surface parameters at different resolutions.

Remote sensing generally identifies only one dominant land-cover type in a pixel but other minor land-cover types are ignored in the derived surface parameters. Remote sensing values generated at coarse resolutions are often the only available data. They are often referred to as lumped data and lumped algorithms (Chen 1999; Hu and Islam 1997). The fact that only one cover type is labeled per pixel at a coarse resolution results in large biases of the final products (Chen et al. 2002). Optimally, the surface variable at a coarse resolution should be calculated from the finer resolution through an aggregation scheme, instead of deriving it from remotely sensed images directly at coarser resolutions. The loss of information with coarsening spatial resolution depends to some degree on the aggregation scheme used. One common approach is to take the average of the fine pixels within each coarse-resolution grid as the representative value for the grid (Simic et al. 2004). Alternative algorithms, such as taking the value at the geographic center point of each large grid to simply represent the value for this grid, also is an option that it sometimes chosen by researchers (Turner et al. 1996). A straight spatial averaging algorithm, however, is inadequate for up-scaling for vegetation type and this is the most important factor in LSMs with regard to regional fluxes because physiological differences such as stomatal/canopy conductance, assimilation rates, etc., strongly influence energy, water, and carbon exchange with the atmosphere (Sellers et al. 1996). As emphasized by Kimball et al. (1999), in large modeling grids, subgrid land-cover characteristics may exert a major control over regional mean fluxes.

b. Spatial scaling algorithms for model coupling

This paper reports the results of incorporating the EASS LSM into the Global Environmental Multiscale model (GEM) GCM (Côté et al. 1998a,b) with two different approaches for handling subgrid heterogeneity. The first approach (lumped case, referred to hereafter as approach L) ignores the variability in subgrid processes (i.e., mainly dependent on the dominant land-cover type) and represents these processes in the GCM with generalized parameters. The second ap-

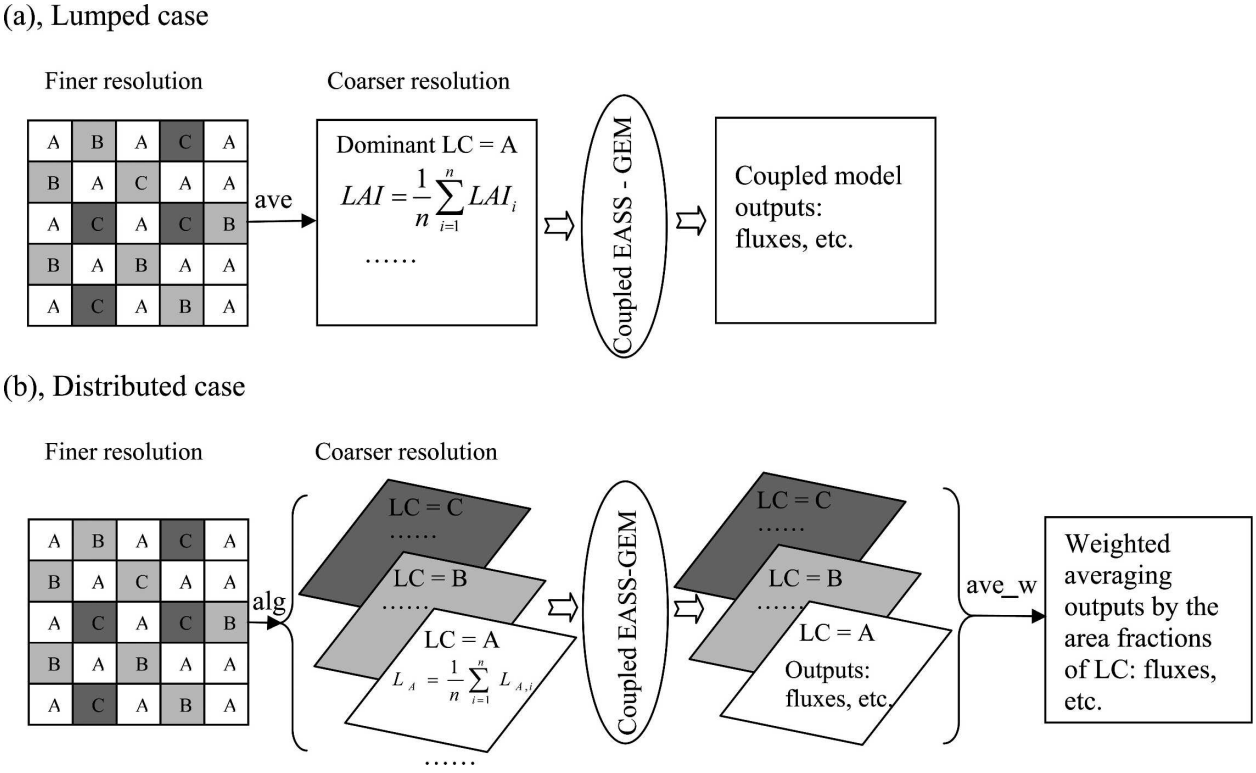

FIG. 1. Schematic diagram for the coupled EASS–GEM model's scaling experiment. (a) Approach L—lumped case: the coarse grid is labeled as one (dominant) land-cover type, while other land surface variables (i.e., LAI, soil properties, etc.) are averaged across all the finescale pixels (e.g., 1 km) within the corresponding coarse grid. (b) Approach D—distributed case: each land-cover type within the coarse grid is considered with one set of algorithms. LC represents land-cover type; *A, B,* and *C*, represent land-cover types for coniferous forest, deciduous forest, and others (including grasses, shrub, etc.), respectively; *L* is leaf area index; alg represents land-cover-type-dependent algorithm; ave is averaging process; ave_*w* is weighted averaging by the area fractions of LC.

proach (distributed case, referred to hereafter as approach D) is based on the belief that subgrid heterogeneous inputs and processes have significant nonlinear effects on processes at GCM scales. Therefore, we should not simply scale up by an aggregating or averaging method.

The two scaling approaches used in this study are outlined in Fig. 1. In approach L (lumped case), the coarse grid in GEM is labeled as one (dominant) land-cover type, while other land surface variables (i.e., LAI, soil properties, etc.) are averaged from all the finescale pixels (i.e., 1 km^2) within the grid. Only one suite of algorithms and physiological parameters specific to that land-cover type (such as vegetation height, displacement height, roughness length, root profile, and biomass) is applied at the large scale (Fig. 1a). In approach D (distributed case), the most sensitive and important variable for land surface schemes and ecological models, that is, land cover, is emphasized. Each land-cover type within a model grid box is considered, and all the input variables related to each specific land-cover type are averaged from all the fine resolution pixels (e.g., 1 km^2) (Fig. 1b). For example, the LAI of land-cover type *B* at *j* grid box ($L_{B,j}$) can be calculated from

$$L_{B,j} = \frac{1}{n}\sum_{i=1}^{n} l_{B,j,i}, \tag{1}$$

where, $l_{B,j,i}$ represents the LAI of land-cover type *B* at pixel *i*, and *n* is the number of those fine pixels within the grid cell *j*. Assuming the effects of lateral interaction on regional fluxes are negligible among pixels within a grid box, the flux representative for the grid cell ($H_{D,j}$) can be calculated by weighting the individual flux ($H_{j,k}$) of land-cover type *k* with the fractional coverage ($f_{j,k}$); that is,

$$H_{D,j} = \sum_{k=1}^{m} H_{j,k} f_{j,k}, \tag{2}$$

where *m* is the total number of cover types in the grid box.

3. Model description

a. The GEM atmospheric model

In this study, the GEM model (Côté et al. 1993, 1998a,b), which has been used for short-range regional forecasting in Canada, is applied to test the two upscaling approaches. In the model, primitive hydrostatic equations are integrated using the semi-implicit and semi-Lagrangian numerical techniques. The model runs on a rotated global variable-resolution grid at a resolution of 0.22° latitude × 0.22° longitude in the central portion of the model grid, which covers North America and the adjacent waters. The vertical resolution is also varying, with a greater concentration of levels in the boundary layer. A terrain-following normalized pressure coordinate is used. The execution time step is 720 s. The embedded surface scheme (ISBA) in GEM is documented in Bélair et al. (2003). ISBA calculates the surface fluxes based on a "big leaf" assumption. The soil column is divided into two layers where temperatures are predicted at the surface (T_s) and subsurface (T_2). The soil water contents are modeled at near surface (first 10 cm, w_g) and rooting depths (w_r). The land surface data are prescribed. ISBA–GEM will produce a set of surface turbulent energy fluxes that will be compared with those simulated by EASS–GEM in section 5.

b. The EASS LSM

The EASS model formulation and test with multiple-year data are described in detail in C07. Major features of the model are briefly described below. (i) The time-varying vegetation parameters such as LAI are derived from satellite data (updated every 10 days) rather than prescribed monthly as in ISBA. (ii) Vegetation cover is treated as a single layer and the model includes a scheme with stratification of sunlit and shaded leaves to minimize the biases from the "big leaf" approximation. A foliage clumping index (Ω), in addition to LAI, is used to characterize the effects of three-dimensional canopy structure on radiation, water, and carbon fluxes. The index Ω is generated from multiple angle remote sensing data. (iii) Energy, water, and carbon are fully coupled and simulated simultaneously. Photosynthesis, evapotranspiration, and stomatal conductance are explicitly linked. The stomatal physiology depends on the photosynthetic response to sunlit/shaded foliage temperature, absorbed photosynthetically active radiation, ambient CO_2 concentration, vapor pressure deficit, soil water, and foliage nitrogen. The decomposition rates of various carbon pools are modified by soil moisture and temperature in different soil layers. Soil carbon dynamics are simulated using a modified soil submodel of CENTURY. (iv) A multilayering scheme for energy exchanges and water transfers through the soil layers and/or snowpack (if present) is introduced in EASS. The number of snow and soil layers and the depth of each layer are user defined according to soil physical structures, snow depth, and application objectives. The soil profile is divided into seven layers and the thickness of the layers increases exponentially from the top layer to the sixth layer (equals to 0.05, 0.1, 0.2, 0.4, 0.8, 1.6 m, respectively). The first six soil layers with a total depth of 3.15 m are set to ensure the complete simulation of energy dissipation in the soil column. The depth of the bottom soil layer is adjusted according to water table depth. The division of soil layers is applied to the snowpack if present. The total depth of snowpack is updated at every time step. When the snowpack is thinner than 5 cm, it is treated as part of the first soil layer and is weighted to obtain the grid cell values. Moreover, the dynamics of snowpack and freeze–thaw cycle in the soil profile are emphasized in EASS since there are large cold regions (e.g., tundra) in Canada (see C07 for details).

EASS is forced by near-surface meteorological variables at a reference level z_{ref} within the atmospheric boundary layer, including surface air temperature (T_{air}), relative humidity (RH), incoming shortwave radiation (R_{in}), wind speed (u), and precipitation (P).

c. Coupling of EASS with GEM

To build communication between these two models, we created an interface program inside GEM through which (i) meteorological fields simulated by GEM are passed to EASS; (ii) preprocessed, remote-sensing-based land surface parameters, treated as inputs to GEM, are transferred to EASS; and (iii) the EASS outputs are passed back to GEM for analysis. The coupled EASS–GEM model (lumped case) takes more computing time by ~8% than the uncoupled GEM while the distributed case takes 3 times more computing time than the lumped one since the EASS model is executed for each land-cover type in each grid cell.

d. Initialization

1) Meteorological variables and soil temperatures/moistures

We run the GEM model with the same configurations and model parameters as in the operational regional forecast, so that the archived operational analysis can be utilized for model initialization. The coupled model is launched for a 24-h integration at 0000 UTC

once a day. The initial atmospheric conditions are provided by a regional data assimilation system (RDAS), with 12-h cycles using trial fields from 6-h regional GEM integrations (Chouinard et al. 1994). The initial surface temperatures and soil water contents at 0000 UTC are derived from a sequential assimilation system based on an error-feedback mechanism. Assuming that the bottom soil layer in EASS is saturated and has the same temperature as the annual mean air temperature, the initial temperature and water content for each soil layer are linearly interpolated from the simulations by ISBA–GEM (i.e., T_s and T_2; w_g and w_r).

2) SOIL CARBON POOLS

The soil carbon stocks are critical to the estimation of respiration. Nine different soil carbon pools are treated as diagnostic parameters in EASS, including two biomass pools (fine root and coarse root), five litter pools (surface structural, surface metabolic, soil structural, soil metabolic, and woody), and two microbial pools (surface microbial and soil microbial). The pool sizes and distributions at 1-km resolution over Canada for 2003 were initialized by the Integrated Terrestrial Ecosystem Carbon-budget model (InTEC V3.0). InTEC V3.0 is a terrestrial carbon dynamics model in yearly time step for the period 1901–2003. It integrates the effects of disturbance and nondisturbance factors on ecosystem carbon balance, such as the effects of nitrogen, climate, stand age, and atmospheric CO_2, etc. (Chen et al. 2000, 2003; Ju and Chen 2005).

4. Dataset for modeling

a. Spatially explicit land surface input dataset

Land surface boundary conditions, including LC, LAI, Ω, soil textures, and carbon pools are required input data for the EASS model. These data are prepared for a spatial domain covering Canada's landmass at 1-km resolution (5700 × 4800 pixels). The domain is in a Lambert conformal conic (LCC) projection. These data are then up-scaled to GEM's grid using algorithms discussed in section 2b.

1) LAND COVER (LC)

As mentioned above, the information on land-cover type is crucial for the coupled model execution and scaling investigation. It is also useful in developing biome-dependent algorithms for the derivation of LAI maps [discussed in section 4b(2)].

The land-cover map of Canada is generated to provide an up-to-date, spatially and temporally consistent national coverage. The data source is the Advanced Very High Resolution Radiometer (AVHRR) on board the National Oceanic and Atmospheric Administration satellite *NOAA-14*. The methodology for data processing and atmospheric correction are documented by Cihlar et al. (1997, 1999) and Liu et al. (2003). The quality of the dataset is assessed by comparing with Landsat Enhanced Thematic Mapper (LETM) images at 30-m resolution. Klita et al. (1998) found the preclass accuracy to vary between 21.8% and 97.9% in a forest region of central Canada. Pietroniro and Soulis (1999) examined this map and other six land-cover maps for the Mackenzie Basin in Canada and ranked this map as having the highest overall accuracy. Some minor cover types have low accuracies at 1-km resolution in comparison with 30-m resolution because of the omission error; that is, small areas disappear when mixed with dominant cover types in large pixels (Liu et al. 2003).

The 31-class land-cover map at 1-km resolution is shown in Fig. 2a. These 31 classes are then reclassified into four groups according to the scaling algorithms discussed in section 2b (Fig. 1). The four groups are coniferous forest, deciduous forest, all other biome types (i.e., grassland, cropland, shrubland, etc.), and nonbiome types (water body and permanent snow/ice area, etc.) (Table1). The dominant land-cover map for these four types at GEM's spatial resolutions (~0.22°) is shown in Fig. 2b. The fractional coverage of the first three groups used for distributed up-scaling (see Table 1) are shown in Fig. 2: c1, c2, and c3, respectively.

→

FIG. 2. Maps of land surface parameters used as the EASS–GEM model inputs for Canada's landmass. (a) Land-cover type at 1-km resolution for the original 31 classes in Cihlar et al. (1999) (see Table 1). (b) Vegetation classification schemes used in the coupled EASS–GEM model (see Table 1), where D, C, O, and N represent coniferous forest, deciduous forest, other biome types, and nonvegetation type, respectively. (c1), (c2), (c3) The fractions of D, C, O, respectively, which are used for the distributed case in EASS–GEM at "gvp22" grid coordinate. The gvp22 is a rotated variable grid coordinate with the finest resolution of 0.22° latitude × 0.22° longitude in the central portion of the model grid, which covers North America and the adjacent waters. (d), (e) The LAI maps at 1-km resolution and in EASS–GEM with gvp22 grid coordinate, respectively. (f), (g) The maps of soil texture types at 1-km resolution and in EASS–GEM with gvp22 grid coordinate, respectively. The numbers 1–11 in the legend in (g) indicate the soil texture types as listed in Table 2.

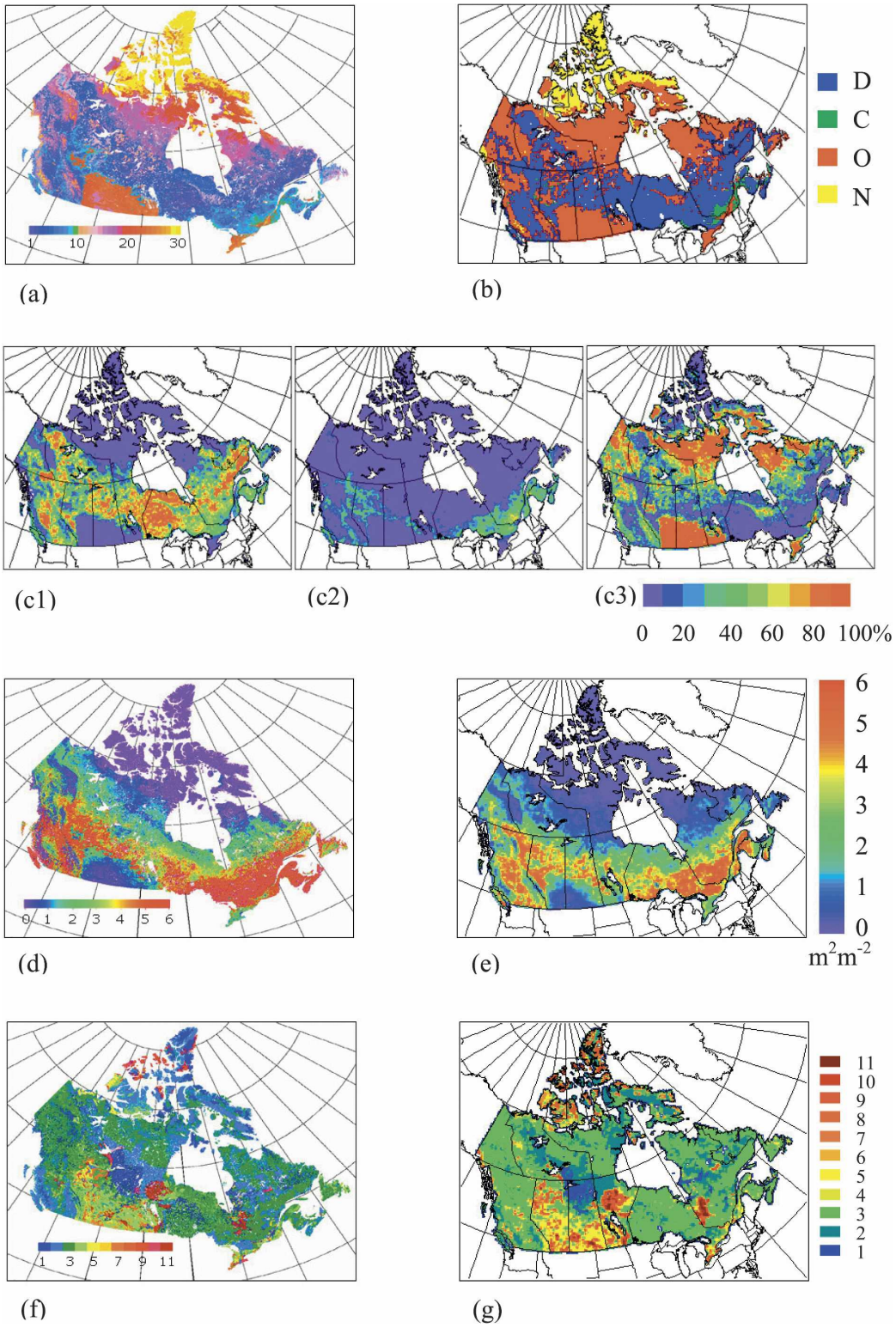
1 10 20 30
(a)
D
C
O
N
(b)
(c1)
(c2)
(c3)
0 20 40 60 80 100%
0 1 2 3 4 5 6
(d)
(e)
6
5
4
3
2
1
0
m2m-2
1 3 5 7 9 11
(f)
(g)
11
10
9
8
7
6
5
4
3
2
1

TABLE 1. Vegetation classification schemes used in EASS–GEM and their correspondence to the original 31 classes in Cihlar et al. (1999).

EASS–GEM	Ciihlar et al. (1999)
Coniferous forest (i)	High density (i); medium density: southern forest (ii); medium density: northern forest (iii); low density: southern forest (iv); low density: northern forest (v); mixed forest: mixed coniferous forest (vi); mixed intermediate forest: mixed uniform forest (vii);* mixed intermediate forest: mixed heterogenous forest (viii)*
Deciduous forest (ii)	Mixed intermediate forest: mixed uniform forest (vii);* mixed intermediate forest: mixed heterogeneous forest (viii);* mixed intermediate: forest mixed broadleaf forest (ix); deciduous broadleaf forest (x)
Other vegetation types (iii)	Burns: low green vegetation cover (xi); burns: green vegetation cover (xii); transition treed shrubland (xiii); wetland/shrubland: high density (xiv); wetland/shrubland: medium density (xv); grassland (xvi); tundra–shrub and lichen dominated: lichen and others (xviii); tundra–shrub and lichen dominated: shrub/lichen dominated (xviii); tundra–treeless: heather and herbs (xix); tundra–treeless: low vegetation cover (xx); tundra–treeless: very low vegetation cover (xxi); cropland: high biomass (xxii); cropland: medium biomass (xxiii); cropland: low biomass (xxiv); mosaic land: cropland–woodland (xxv); mosaic land: woodland–cropland (xxvi); mosaic land: cropland–other (xxvii)
Nonvegetation type (iv)	Bare soil and rock (xxviii); urban and built-up (xxix); nonvegetated land: water (0); nonvegetated land: snow/ice (xxx)

* We treated the types (vii) and (viii) in Cihlar et al. (1999) as half coniferous forest (i) and half deciduous forest (ii) in EASS–GEM.

2) LEAF AREA INDEX

The LAI images of 1-km resolution for the period of August 2003 for Canada (Fig. 2d) are generated from the 10-day composite VEGETATION images using a cover type-based algorithm (Chen et al. 2002). In approach L, LAI for each GEM grid box is simply averaged from all fine pixels (Fig. 2e). In approach D, LAI for each land-cover type in GEM model's grid is calculated using Eq. (1) from 1-km data.

3) SOIL TEXTURE DATA

The soil textural data (silt and clay fraction) and dissolved organic matter (DOM) data for each EASS soil layer are taken directly from Soil Landscapes of Canada (SLC) version 2.0 (Tarnocai 1996; Shields et al. 1991; Schut et al. 1994; Lacelle 1998). For soil depths where there is no default data, the value of the layer immediately above is used. To generate these data layers with the same projection and resolution as for other data layers, the original vector data in SLC are mosaicked, reprojected, and rasterized using the ARC/INFO geographic information system (Chen et al. 2003).

Soil texture is crucial to soil properties, such as soil water content at saturation (porosity), soil water potential at saturation, soil heat and hydraulic conductivities at saturation, etc. To determine the hydraulic and physical properties of the soil layers, we classify soil texture classes into 11 categories following Campbell

TABLE 2. Soil types and model parameters used in EASS–GEM.*

Texture types	Sand (%)	Silt (%)	Clay (%)	b	$K_s \times (10^{-3}$ m s$^{-1})$	ϕ m^3 (m^{-3})	θ_{sat} (m^3 m^{-3})	θ_{wlt} (m^3 m^{-3v})	ψ_e (m H_2O)
Sand (i)	0.92	0.05	0.03	1.7	5.80	0.437	0.09	0.03	0.7
Loamy sand (ii)	0.81	0.12	0.07	2.1	1.70	0.437	0.13	0.06	0.9
Sandy loam (iii)	0.65	0.25	0.10	3.1	0.72	0.453	0.21	0.10	1.5
Loam (iv)	0.42	0.40	0.18	4.5	0.37	0.463	0.27	0.12	1.1
Silty loam (v)	0.20	0.65	0.15	4.7	0.19	0.501	0.33	0.13	2.1
Sandy clay loam (vi)	0.60	0.13	0.27	4.0	0.12	0.398	0.26	0.15	2.8
Clay loam (vii)	0.32	0.34	0.34	5.2	0.064	0.464	0.32	0.20	2.6
Silty clay loam (viii)	0.09	0.58	0.33	6.6	0.042	0.471	0.37	0.32	3.3
Sandy clay (ix)	0.53	0.07	0.40	6.0	0.033	0.43	0.34	0.24	2.9
Silty clay (x)	0.10	0.45	0.45	7.9	0.025	0.479	0.39	0.25	3.4
Clay (xi)	0.20	0.20	0.60	7.6	0.017	0.475	0.40	0.27	3.7

* In the table, b is the exponent of the moisture release equation (Campbell and Norman 1998); K_s is the saturated hydraulic conductivity of the soil; ϕ is the soil porosity; θ_{sat} and θ_{wlt} are the soil moisture content at field capacity (33 J kg $^{-1}$) and the wilting point (1500 J kg^{-1}), respectively; and ψ_e is the air entry potential. All values are after Campbell and Norman (1998) except ϕ, which is after Kucharik et al. (2000).

TABLE 3. Description of the tower sites used for model–data comparison and the vegetation-type composites within the EASS–GEM coupled model grid containing a given tower.

No. and name	Location	Elevation	Vegetation type		Province
			Site descriptions	EASS–GEM*	
Site 1: 1948 Douglas fir stand	49.905°N, 125.366°W	320 m	54-yr-old Douglas fir with 17% red cedar and 3% western hemlock	(i) 45%; (ii) 43%; (iii) 1%	BC
Site 2: Old aspen	53.629°N, 106.197°W	600 m	83-yr-old mature aspen with a few balsam poplar, thick hazel	(i) 44%; (ii) 54%; (iii) 2%	SK
Site 3: Old jack pine	53.916°N, 104.692°	579 m	91-yr-old mature jack pine, very sparse green alder, predominantly lichen ground cover	(i) 76%; (ii) 7%; (iii) 17%	SK
Site 4: CPRS (black spruce/jack pine cutover)	49.267°N, 74.036°W	961 m	Regenerating black spruce, Vaccinium *spp*., ledum, moss	(i) 51%; (ii) 5%; (iii) 41%	QC
Site 5: Nashwaak Lake site 01	46.472°N, 67.100°W	341 m	Mature balsam fir forest: composed of predominantly balsam fir of 32–37 yr old	(i) 47%; (ii) 45%; (iii) 8%	NB

* The composite of land-cover types for the particular EASS–GEM pixel surrounding the tower site, where (i), (ii), and (iii) are coniferous forest, deciduous forest, and other biome type, respectively.

and Norman (1998), Rawls et al. (1992), and Kucharik et al. (2000). These 11 categories and their hydraulic and physical coefficients are listed in Table 2. The soil texture maps for Canada at 1 km and at GEM's spatial resolutions are shown in Figs. 2f and 2g, respectively.

b. Site data for model comparison

Canada's southern forest regions are comprised of a mosaic of both forests and peatland ecosystems. Five flux stations across an east–west transect over these regions, maintained by Fluxnet-Canada, are selected for model validation in this study. These five sites are briefly described in Table 3. The land surface input data for the grid box surrounding the tower sites are also included in Table 3.

Since EASS is driven by meteorological fields modeled by GEM, the biases in GEM will cause biases in the EASS simulated fluxes. To correctly assess EASS model performance, the modeled meteorological variables are also compared with tower observations.

5. Results and discussion

a. Model comparisons with measurements from five flux tower sites

1) SURFACE SOLAR RADIATION AND METEOROLOGY

The incoming solar shortwave radiation data were not available for site 4 (CPRS: black spruce/jack pine Cutover, Quebec, Canada). The GEM-simulated hourly R_{in} data were found to reasonably follow the observations for all the other four sites. The squared linear regression coefficient (r^2) and the root-mean-square error (RMSE) equaled 0.71 and 151.67 W m^{-2}, respectively (Table 4). The tower-observed and simulated 7-day composite diurnal variations of meteorological variables (R_{in}, T_{air}, RH, and u) for all the five sites are first compared in Fig. 3. The linear regression results between tower observed and simulated meteorological variables are listed in Table 4. Modeled T_{air} explained 78.8% of tower observations. The bias between simulated and observed RH was 15%–80%, whereas it was over 30%–100% for u. RH was underestimated while u was overestimated at all five towers most of the time, and T_{air} was underestimated at site 1 although it was overestimated at site 5. Overall, the differences of the biases were very small among the five sites (Fig. 3). The

TABLE 4. Relationship between GEM-modeled and tower-observed hourly meteorological variables for all five sites.*

	r^2	Slope (m)	Interception (b)	RMSE	Sample number (n)
R_{in}**	0.71	0.89	78.67	151.67 (W m^{-2})	544
T_{air}	0.79	0.98	0.47	2.58 (°C)	840
RH	0.71	0.56	5.04	24.54 (%)	840
u	0.35	0.79	2.25	2.26 (m s^{-2})	820

* The linear equation used here is $y_{mod} = m \times x_{obs} + b$; r^2 is the squared linear regression coefficient; RMSE is the root-mean-square error $= \sqrt{(1/N)\Sigma_{i=1}^{N}[C_{mod}(i) - C_{obs}(i)]^2}$.

** R_{in} is the total incoming global shortwave radiation; T_{air}, RH, and u are the air temperature, relative humidity, and wind speed above canopy, respectively.

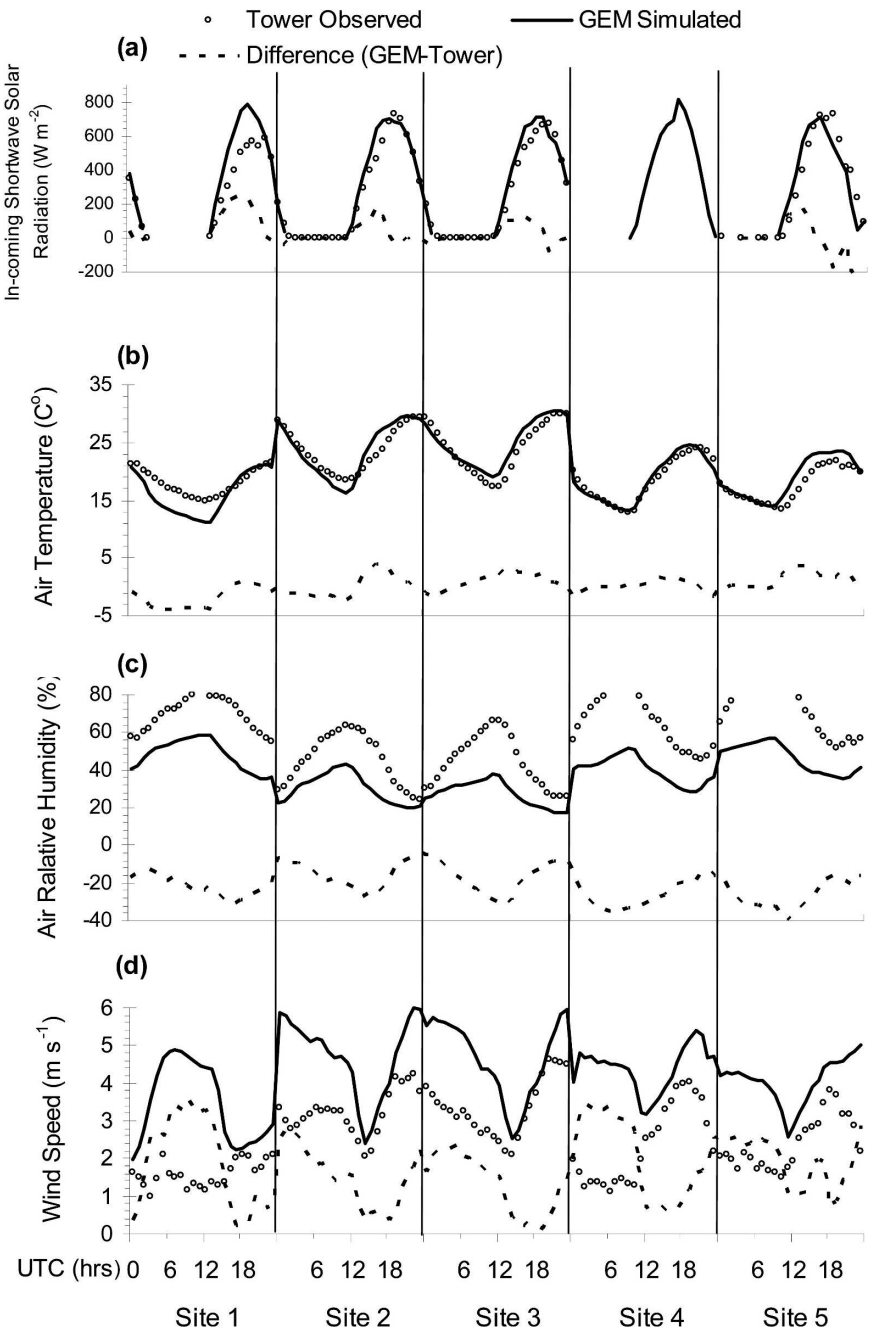

FIG. 3. Comparisons of the GEM-simulated 7-day composite diurnal variations in several meteorological variables with the tower observations during 13–19 Aug 2003 for all five sites for (a) R_{in}, (b) T_{air}, (c) RH, and (d) u. The solid line is the GEM simulated, the symbol is observed from the tower, and the dashed line is the difference between simulations and observations.

simulated hourly meteorological data during 13–19 August 2003 are compared with tower measurements at site 2 as an example (Fig. 4). Overall, considerable biases exist between GEM modeled and tower-observed hourly meteorological variables (Table 4).

2) FLUXES

The model grid box in EASS–GEM (~24 × 24 km^2) is much larger than the tower flux footprint area (normally 1~2 km^2). Except for sites 3 and 4, the vegetation

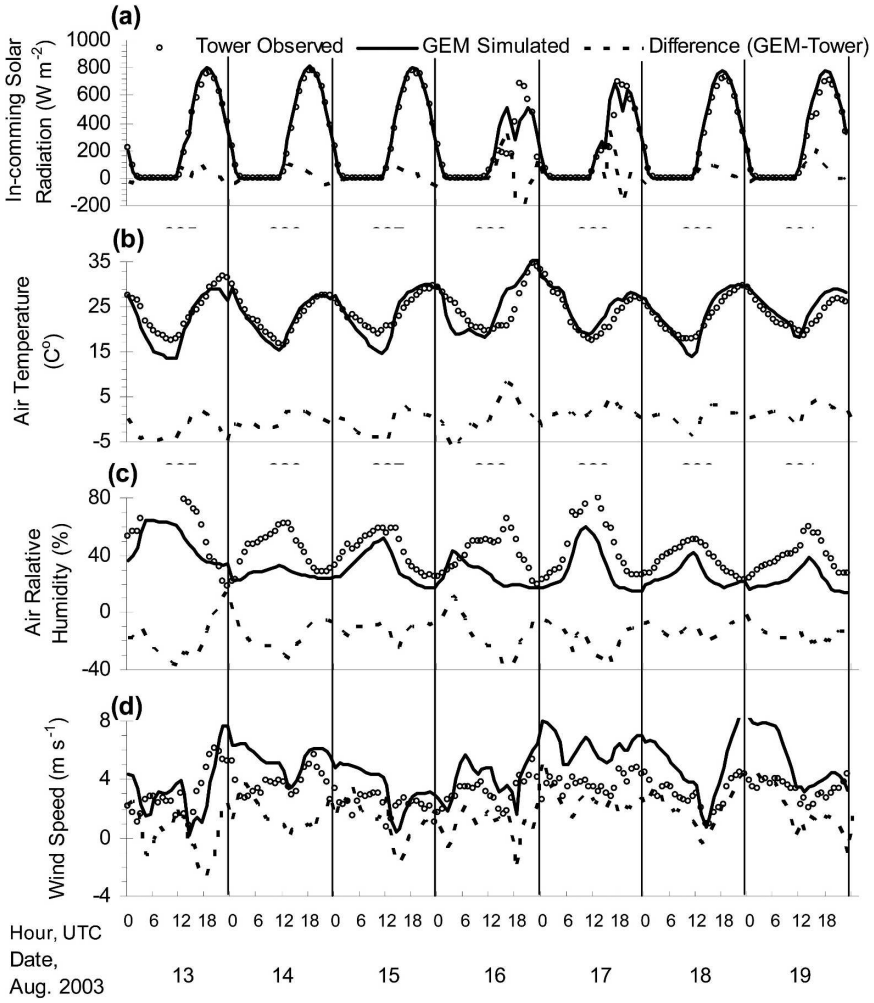

FIG. 4. Comparisons of the GEM-simulated diurnal variations in several meteorological variables with the tower observations during 13–19 Aug 2003, for site 2: (a) for R_{in}, (b) for T_{air}, (c) for RH, and (d) for u. The solid line is GEM simulated, the symbol represents tower observed, and the dashed line is the differences between simulations and observations.

type within the flux footprint area for the other three towers is consistent with the dominant vegetation type of the grid box containing the particular tower (Fig. 5). For comparison with the tower observations, we present results using only approach L (dominant land-cover case) for our model simulations. There was little difference between approaches L and D.

The surface fluxes simulated by the EASS–GEM and ISBA–GEM models and measured at site 2 during 13–19 August 2003 are compared in Fig. 6. It appears that the EASS–GEM model captured about 94%, 73%, 84%, and 64% of the hourly variations in tower observations of net solar radiation (R_n), latent heat flux (λE), sensible heat flux (H), and net ecosystem exchange of CO_2 (NEP) at site 2, respectively; whereas the ISBA–GEM model only explained 59% and 47% of observed λE and H. Overall, the model results show that both the EASS–GEM and ISBA–GEM models have the capacity of reasonably capturing the observed diurnal variations in the surface fluxes for all five sites (Table 5; Figs. 6 and 7), but the model biases are still considerable. The sensible heat flux is underestimated by around 10% in EASS–GEM and by 20%–60% in ISBA–GEM comparing with the tower observations. The latent heat flux is overestimated by both models (except at site 5 by ISBA–GEM). The biases in simulated surface fluxes are also site dependent. The largest bias in simulated NEP by the EASS–GEM model was found at site 3 (Fig. 7; Table 5), probably because of the inconsistency between the vegetation type in the tower flux footprint area and the dominant vegetation type of the model grid box (Fig. 5).

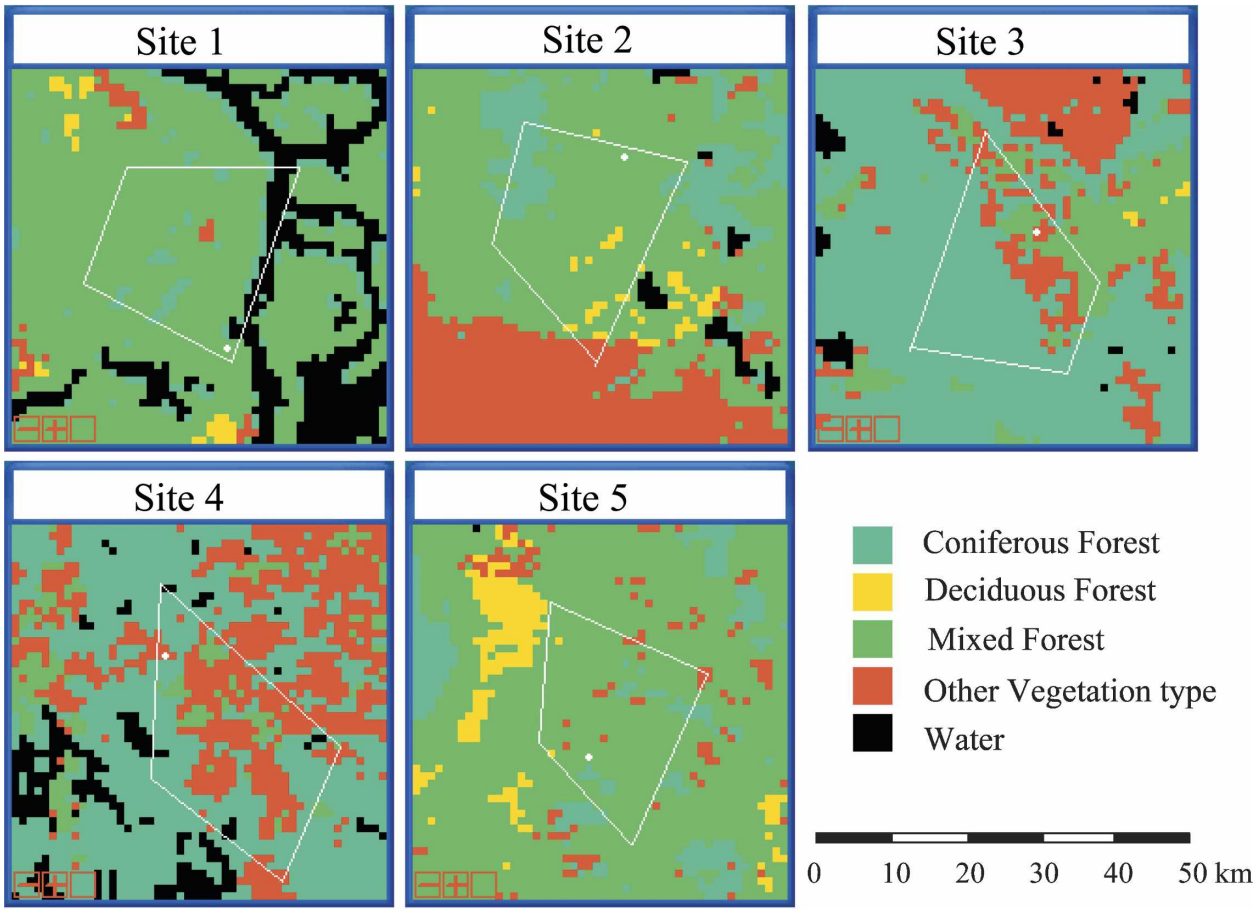

FIG. 5. Land-cover maps in the 50 km × 50 km domain around each observed tower at 1-km resolution. For each panel, the white point indicates the location of the tower and the area within the white quadrilateral roughly represents the model grid in EASS–GEM (a rotated grid coordinate at the resolution of 0.22° latitude × 0.22° longitude) that contains the tower.

Model comparisons demonstrated that the improvements in simulating latent and sensible heat fluxes in the EASS–GEM system are more noticeable than in GEM. Both the land surface input data and the model algorithms in EASS may have contributed to these improvements. The key land surface parameters (i.e., LC, LAI) used in the coupled model are derived from high-spatial-resolution satellite images instead of being prescribed as in ISBA. It has been shown in an earlier study that remotely sensed LC and LAI data are important for modifying the surface fluxes and are most useful for improving the description of spatial variability (Oleson and Bonan 2000). The more advanced algorithms in EASS relative to ISBA could be another reason for the better simulated fluxes. These include the stratification of sunlit and shaded leaves versus the "big leaf" approximation; fully coupled calculation of energy, water, and carbon versus excluding carbon calculation; and a multilayering soil scheme versus the simple two-layer scheme.

The regression analyses between tower observations and model simulations by approaches L and D for all of the five sites are also compared in Table 5. Which upscaling technique yields better agreement with tower measurements is dependent on the consistency in land surface parameters (i.e., LC and LAI) between the tower flux footprint area and the grid box cell surrounding the particular site. In cases when the dominant land-cover types near sites 1, 2, and 5 are consistent with that in the grid box (Fig. 5), the simulated fluxes in the lumped case are slightly more realistic than in the distributed case (Table 5). In contrast, the land covers in the vicinity of towers 3 and 4 are more heterogeneous than towers 1, 2, and 5 (Fig. 5), so the simulations by approach D are closer to observations than by approach L (Table 5).

The distributed technique is expected in theory to have more scaling accuracy in the surface fluxes than the lumped method though the possibilities for verification are limited in practice by the fact that the GEM's

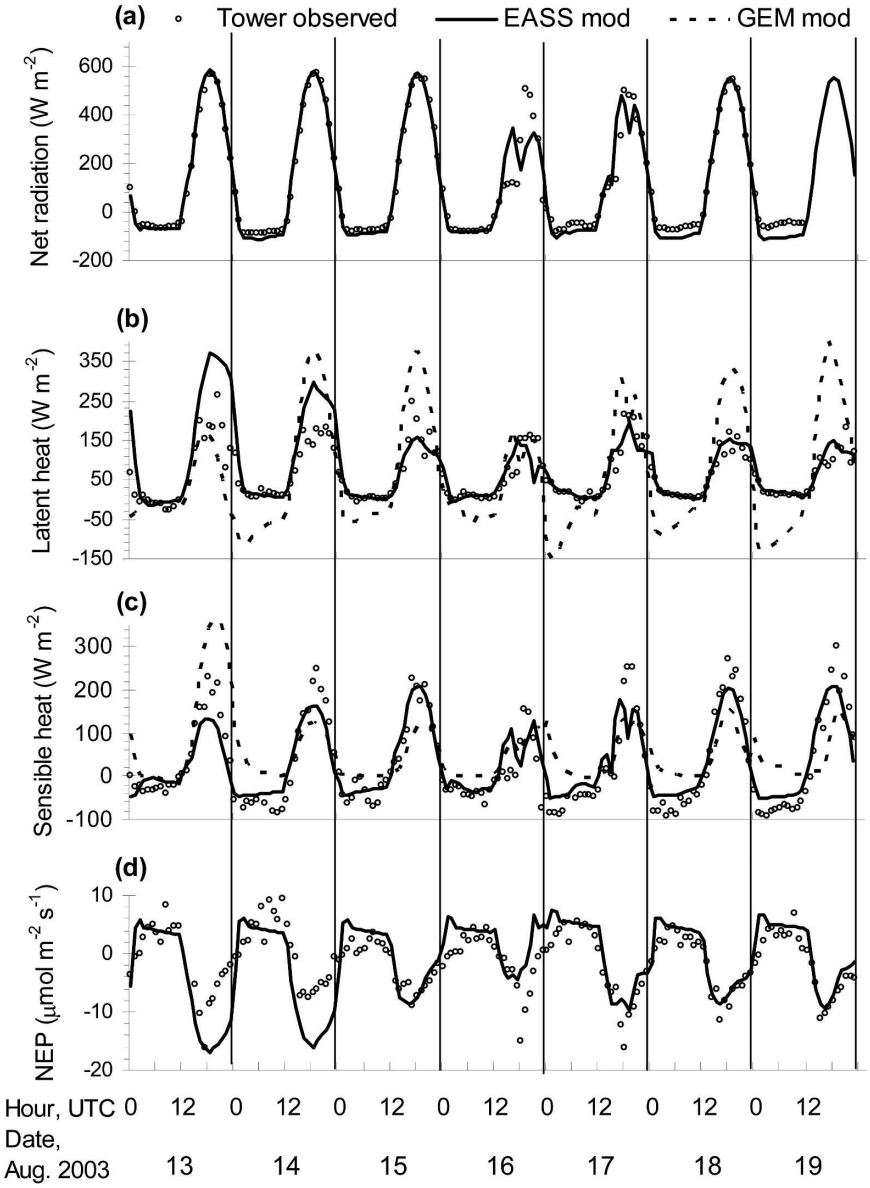

FIG. 6. Comparisons of diurnal variations in energy and carbon fluxes simulated by the EASS–GEM model (approach L) with the tower observations and with ISBA–GEM simulations during 13–19 Aug 2003 for site 2: (a) for R_n, (b) for λE, (c) for H, and (d) for NEP. The solid and dashed lines are modeled using EASS and GEM, respectively, while the symbol represents tower observations.

grid is much larger (up to two to three orders of magnitude) than the eddy flux footprint area. Similar upscaling techniques have been applied to spatial scaling of net primary productivity (NPP). It was found that the lumped calculations of NPP can be considerably biased from the distributed case by up to 15% (Simic et al. 2004). In the current study, the differences in simulated surface fluxes between the two approaches are found to be dependent on the land surface heterogeneities within the GEM's coarse grid cell with a range of 5%–15% (Fig. 8; Table 3). It appears that the minimum difference in energy and carbon fluxes between these two approaches occurred at site 3, where the dominant vegetation type of coniferous forest is over 76%. Among the five sites, the largest difference in energy fluxes was found for the model grid where the land-cover type 3 (i.e., "other" biome type) had the largest fractional coverage (i.e., site 4, more than 40%; see

TABLE 5. Regression relationship between modeled (by the GEM model, which was either coupled or not coupled to EASS) and observed fluxes for all five sites.*

		R_n		LE		H		NEP	
	Model	r^2	RMSE	r^2	RMSE	r^2	RMSE	r^2	RMSE
Site 1	EASS_D	0.85	103.2	0.64	37.1	0.67	62.1	0.67	6.8
	EASS_L	0.86	88.8	0.63	31.7	0.67	66.9	0.68	6.2
	ISBA	N/A	N/A	0.56	72.0	0.69	79.2	N/A	N/A
Site 2	EASS_D	0.93	65.6	0.72	37.8	0.84	44.8	0.61	4.2
	EASS_L	0.94	55.7	0.73	39.4	0.84	45.9	0.64	4.1
	ISBA	N/A	N/A	0.59	105.3	0.47	81.7	N/A	N/A
Site 3	EASS_D	0.93	68.5	0.62	28.5	0.76	92.0	0.37	2.7
	EASS_L	0.94	56.1	0.61	29.7	0.75	92.2	0.36	2.6
	ISBA	N/A	N/A	0.52	127.9	0.59	116.9	N/A	N/A
Site 4	EASS_D	0.83	94.4	0.89	38.9	0.61	69.8	0.51	2.1
	EASS_L	0.82	124.3	0.88	29.8	0.59	81.1	0.50	2.9
	ISBA	N/A	N/A	0.81	78.5	0.58	53.1	N/A	N/A
Site 5	EASS_D	0.78	112.4	0.80	49	0.57	98.6	0.53	6.8
	EASS_L	0.78	108.1	0.79	51	0.58	91.2	0.55	6.2
	ISBA	N/A	N/A	0.45	111.3	0.68	81.6	N/A	N/A
All five sites	EASS_D	0.88	91.2	0.79	36.5	0.65	79.3	0.58	4.8
	EASS_L	0.87	102.4	0.78	39.9	0.66	81.5	0.59	4.9
	ISBA	N/A	N/A	0.52	101.1	0.46	85.3	N/A	N/A

* EASS_L and EASS_D represent approach L (lumped case) and approach D (distributed case); R_n is net shortwave radiation (W m^{-2}), λE is latent heat flux (W m^{-2}), H is sensible heat flux (W m^{-2}) and NEP (μmol m^{-2} s^{-1}) is net CO_2 flux, r^2 is the squared linear regression coefficient, RMSE = $\sqrt{(1/N)\Sigma_{i=1}^{N}[C_{\text{mod}}(i) - C_{\text{obs}}(i)]^2}$, and the sample number for an individual tower is around 150–170 and for all five sites is 780–830.

Table 3 and Figs. 5 and 8), while the biggest absolute difference in carbon flux occurred for the pixels where land-cover type 3 (i.e., "other" biome type) had the smallest coverage (e.g., sites 1 and 2, less than 1%–2%; see Table 3 and Figs. 5 and 8). This may be because the magnitude of carbon flux for cover types 1 or 2 is usually 2–3 times larger than that for cover type 3 (see also Fig. 7; comparing sites 1 or 2 with sites 3 or 4). The relative difference between the two approaches in carbon flux is still dependent on the land surface heterogeneity within the model grid box.

b. *Model comparison with approaches L and D and scaling to Canada's landmass*

The one-week EASS-simulated sensible and latent heat fluxes over Canada for the two approaches and their differences are shown in Fig. 9. There are marked spatial variations in H and λE. It appears that the EASS model may have the overall ability to capture the combined effects of meteorology, vegetation, and soil on spatially distributed patterns of H and λE. Comparison of the simulated distributions of H and λE with maps of land surface parameters (Fig. 2) suggests that the spatial patterns of both H and λE correspond mainly to the distribution of cover types, LAI, and soil texture. Moreover, λE is also controlled by available solar energy and soil moisture conditions. The differences in H and λE between the two approaches are related to spatial heterogeneities in cover types, soil texture, and soil moisture conditions. For example, the largest differences in H and λE between the two approaches were found in northern Manitoba, Saskatchewan, and the west-central regions of the Mackenzie River basin (Figs. 9c and 9f) where the coniferous forest is heavily mosaicked with other cover types (Figs. 2a and 2b). The biases in simulated fluxes could reach ±20% in these regions.

Spatial variability in simulated net radiation (R_n) is smaller than H and λE for most regions (Figs. 10a and 10b). The patterns of the differences in R_n between the two approaches (Fig. 10c), however, are similar to that of H and λE (Figs. 9c and 9f), corresponding to spatial heterogeneities in cover types and soil texture.

Canada-wide maps of carbon sources and sinks simulated by the two approaches are shown in Figs. 10d and 10e, respectively. There are moderate spatial variations in NEP over most regions. The spatial patterns of NEP are mainly influenced by the distribution of vegetation-cover types and LAI. Most carbon sinks correspond to coniferous and deciduous forest-cover types located in the southwestern and southeastern Canada, whereas the mostly carbon-balanced or small source areas

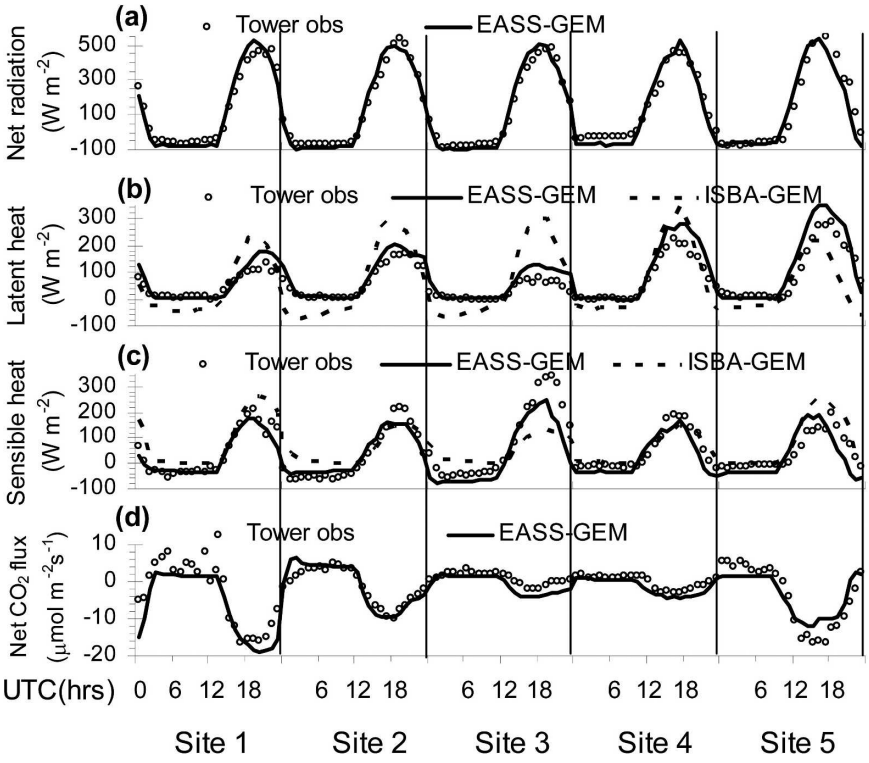

FIG. 7. Comparisons of the 7-day averaging of the diurnal cycles in energy and carbon fluxes between simulations and tower observations during 13–19 Aug 2003 for all five sites: (a) for R_n, (b) for λE, (c) for H, and (d) for NEP. The solid and dashed lines are modeled by EASS–GEM (approach L) and by ISBA–GEM, respectively; the symbol represents tower observations (tower obs).

match the distribution of other biome cover types, which are in northern Canada and in southern Manitoba and southern Saskatchewan (Figs. 10d and 10e). The large differences between approaches L and D mostly occurred near the boundaries between forest and nonforest types (Fig. 10f). In the lumped case, the model could overestimate carbon sources or underestimate sinks by more than 20%–25% in these heterogeneous regions. We also notice that the differences between the weekly composite fluxes by these two approaches may be dampened due to temporal averaging.

The EASS-simulated variables, such as canopy temperature (T_c) and soil surface temperature (T_{s0}) are shown in Fig. 11. The spatial variability in T_c and T_{s0} is not as significant as for the surface fluxes. The differences in T_c and T_{s0} between approaches L and D are similar to that of simulated heat fluxes in spatial distribution and magnitude.

6. Summary

A new distributed LSM, the Ecosystem–Atmosphere Simulation Scheme (EASS), was evaluated for simulating coupled energy, water, and carbon fluxes. Through the use of remote sensing and ancillary data, we coupled EASS with the Global Environmental Multiscale model (GEM) GCM and applied it to test two scaling approaches for handling subgrid heterogeneity (clumped case and distributed case). The coupled experimental runs for a week in August 2003 over Canada provided an opportunity to assess model performance and to investigate the spatial scaling issue. After validating the coupled EASS model with five available sets of flux tower observations over Canada's southern forest regions, the model was demonstrated to have the capacity of reasonably capturing both spatial and temporal patterns in carbon and energy fluxes. However, there were still some significant biases in λE and H between simulations and tower observations. The sensible heat flux was underestimated while the latent heat flux was overestimated by both the EASS–GEM and ISBA–GEM models. The biases possibly result from (i) a combination of errors in models and in eddy covariance measurements; (ii) the difference between the eddy flux footprint area and the model grid cell; and (iii) the biases between the

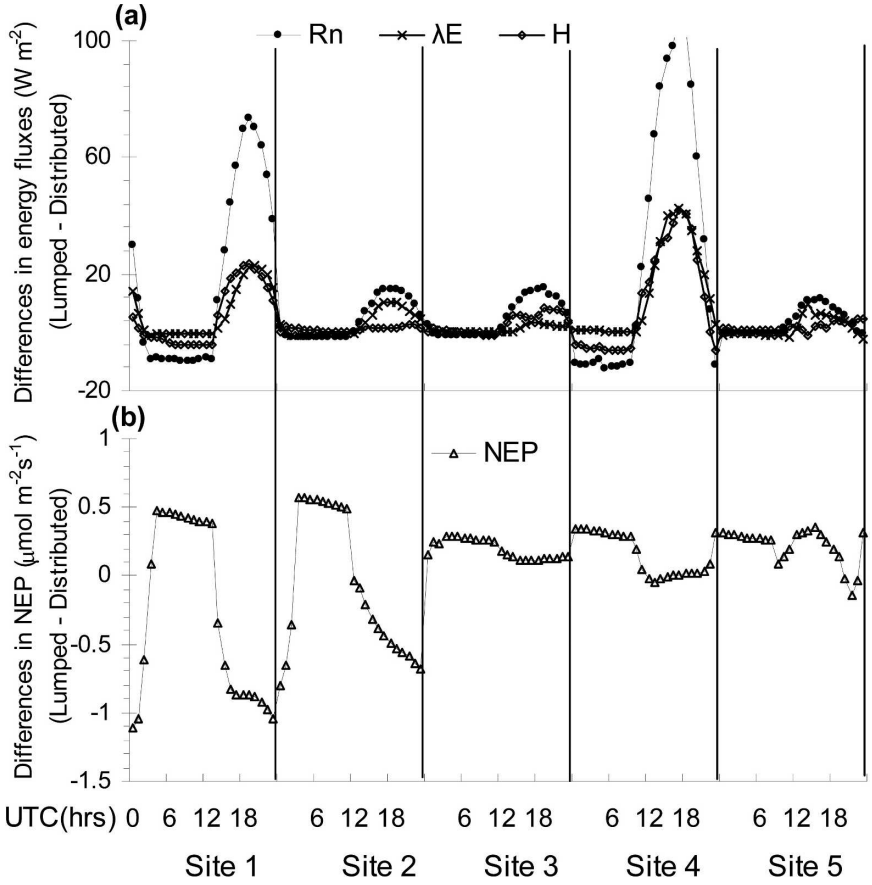

FIG. 8. The differences in simulated 7-day composite diurnal variations in energy and carbon fluxes between approaches L and D in EASS during 13–19 Aug 2003: (a) energy fluxes; (b) net ecosystem exchange of CO_2.

meteorological data simulated by GEM and those observed.

The improvements in simulated latent and sensible heat fluxes in the coupled EASS–GEM system were more noticeable than in the uncoupled GEM (r^2: 0.79 versus 0.52 for latent heat and 0.66 versus 0.46 for sensible heat, respectively; RMSE: 36.5 versus 101.1 W m^{-2} for latent heat and 79.3 versus 85.3 W m^{-2} for sensible heat, respectively). These improvements are thought to be mainly due to the addition of the remotely sensed land surface inputs and the advanced algorithms in EASS compared to the prescribed inputs and simpler algorithms in ISBA used in the uncoupled GEM.

The degree of agreement between model simulations using approaches L and D with eddy flux measurements was also site dependent. It depended on the differences in land surface heterogeneities between the eddy flux footprint area and the model grid cell surrounding the particular tower site. The grid cell in GEM is two to three orders of magnitude larger than the eddy flux footprint area, so this kind of comparison is not ideal or even not satisfactory for model validation. The distributed technique is expected in theory to have more scaling accuracy in estimating of the surface fluxes than the lumped method, which is consistent with the conclusion from a scaling study on NPP using a similar technique.

There were marked spatial variations in H and λE, and comparatively moderate spatial variations in NEP over Canada's landmass. These patterns of spatial variation closely followed patterns of vegetation-cover types and LAI, both of which were highly correlated with the underlying soil texture types. Moreover, it was found that λE was also controlled by available incoming solar radiation and soil moisture conditions, while NEP was additionally affected by the soil carbon pools. The differences in the simulated surface fluxes between the lumped and distributed cases were statistically significant for Canada's landmass ($p < 0.01$ using a t test).

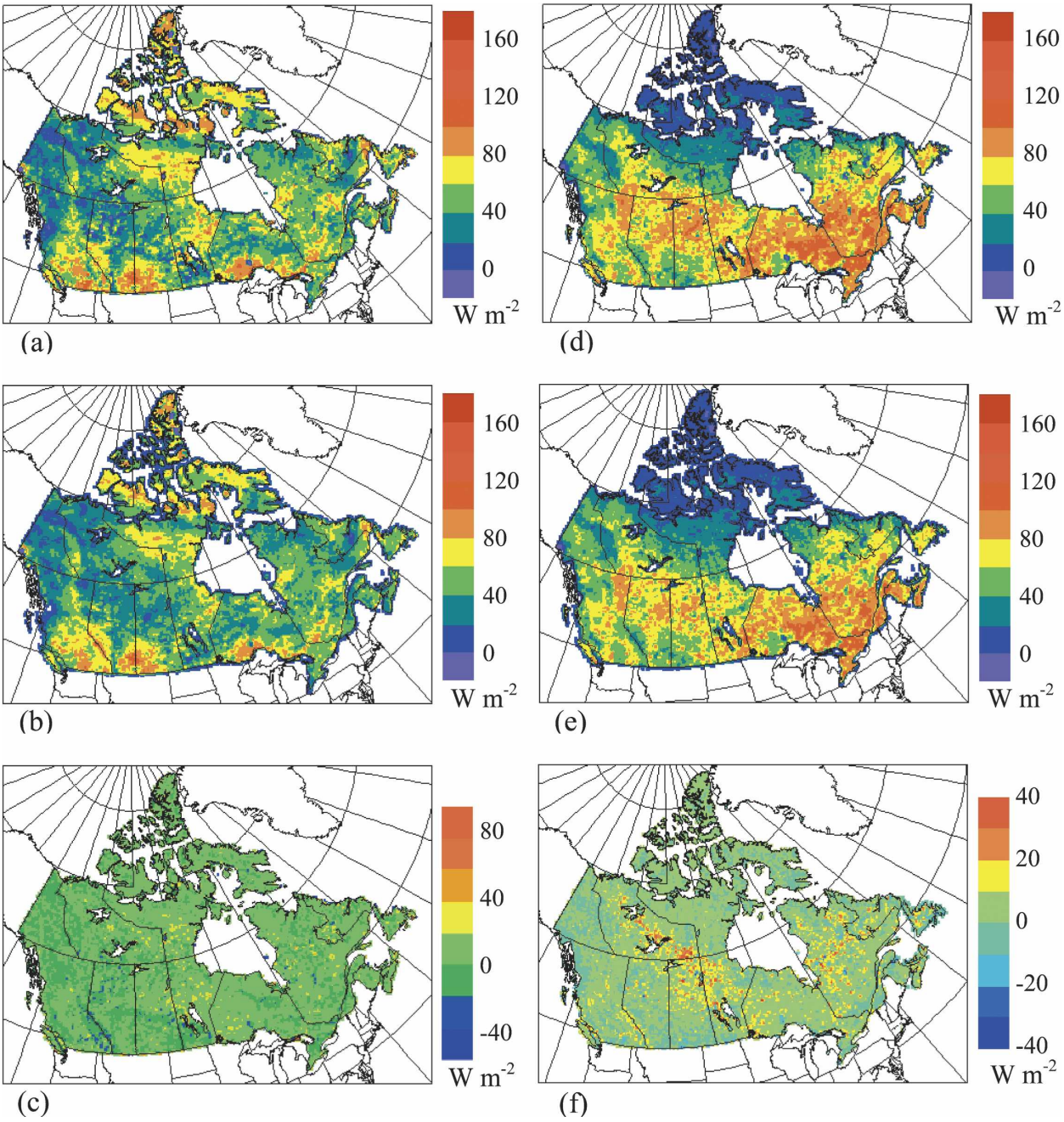

FIG. 9. Maps of surface latent and sensible heat fluxes averaged for 7 days in August 2003 in gvp22 grid coordinate using the coupled EASS–GEM model. (a) The weekly averaged value for the surface sensible heat flux by approach L (lumped case). (b) Same as in (a) but for approach D (distributed case). (c) The difference between these two approaches (lumped minus distributed). (d), (e), (f) Same as in (a), (b), (c), respectively, but for latent heat.

The maximum magnitude of the difference in simulated fluxes between these two approaches ranged from ±10% to ±25% of its absolute value, suggesting that different ways of treating the subgrid's land surface heterogeneities could lead to noticeable biases. The distributions in these maximum biases resulting from the simple lumped case were closely related to heterogeneities in cover types, LAI, and soil texture. The surface fluxes modeled by the two up-scaling approaches (lumped and distributed cases) differed by 5%–15% on average and by up to 15%–25% in highly heterogeneous regions. This suggests that different ways of

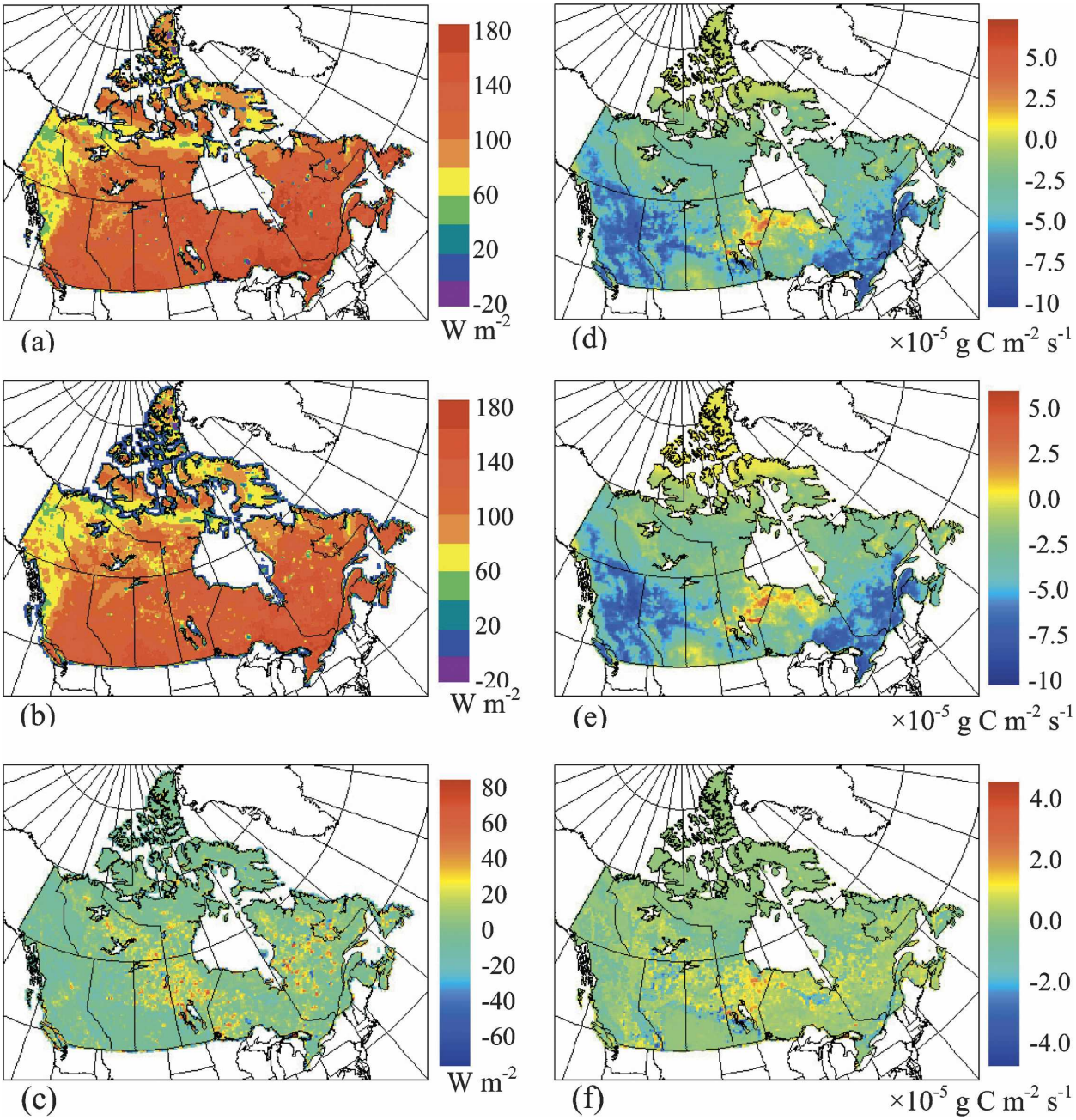

FIG. 10. Maps of 7-day averaged net radiation (R_n) and net ecosystem exchange of CO_2 (NEP) in August 2003 at gvp22 grid coordinate using the coupled EASS–GEM model. (a) The 7-day-averaged value for R_n by approach L (lumped case). (b) Same as in (a) but for approach D (distributed case). (c) The difference between these two approaches (lumped minus distributed). (d), (e), (f) Same as in (a), (b), (c), respectively, but for NEP.

treating subgrid land surface heterogeneities could lead to noticeable biases in model output. In theory, the distributed case should be expected to give moderate improvement in up-scaling of fluxes.

Acknowledgments. This work was supported by the Canadian Foundation for Climate and Atmospheric Sciences (Project GC423). We would like to acknowledge the investigators of the Fluxnet Canada project for the various datasets used in this investigation, Alan Barr (Meteorological Service of Canada), T. Andrew Black (University of British Columbia), Carole Coursolle and Marc-André Giasson (Université Laval), and Charles P.-A. Bourque

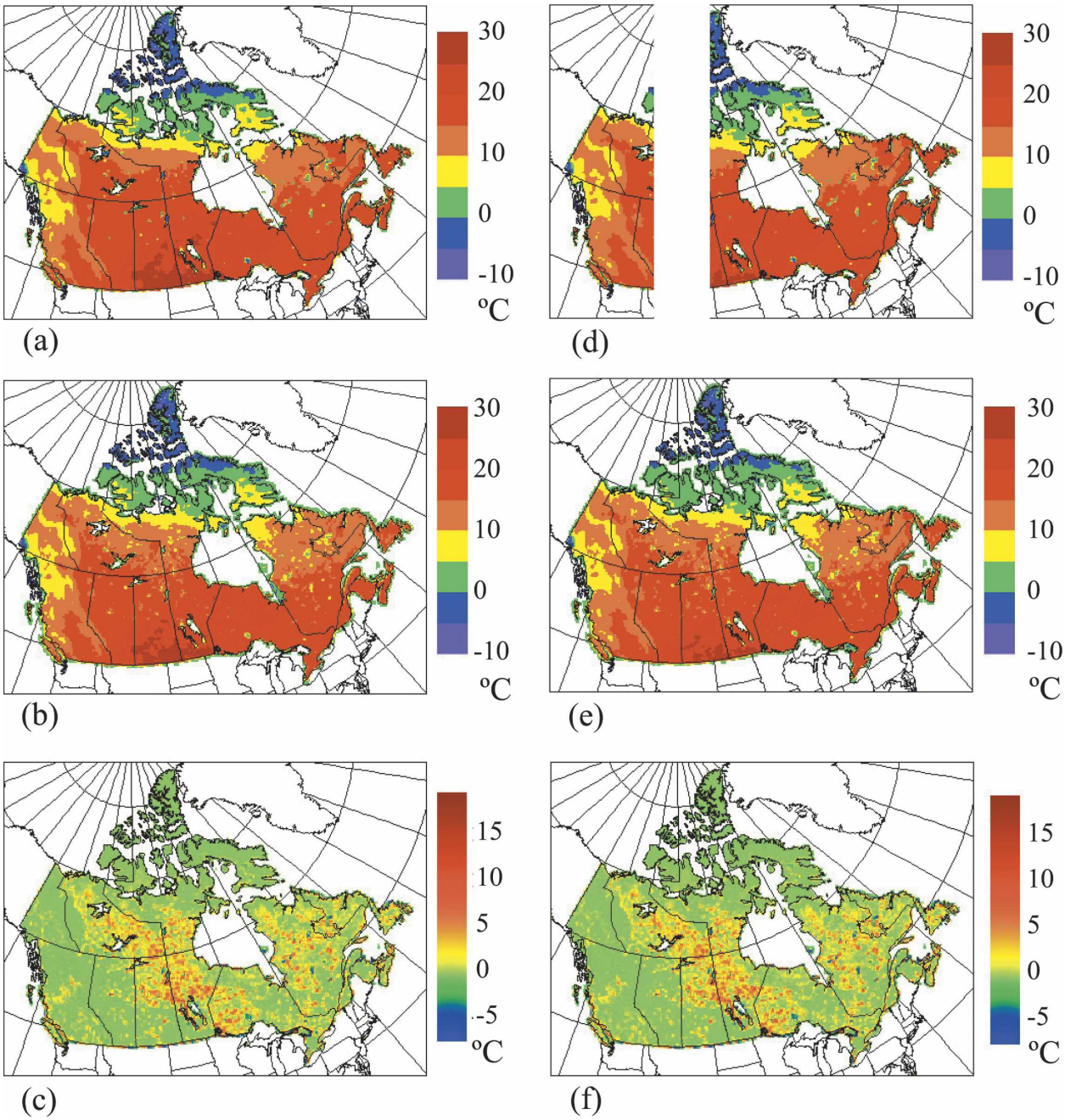

FIG. 11. Maps of a week-averaged canopy temperature (T_c) and soil surface temperature (T_{s0}) in August 2003 at gvp22 grid coordinate using the coupled EASS–GEM model. (a) The 7-day-averaged value for T_c by approach L (lumped case). (b) Same as in (a) but for approach D (distributed case). (c) The difference between these two approaches (lumped minus distributed). (d), (e), (f) Same as in (a), (b), (c), respectively, but for T_{s0}.

(University of New Brunswick). We thank Jane Liu (Department of Physics, University of Toronto, Canada), and Lin Huang and Alexander Shashkov of the Meteorological Service of Canada for useful discussions on early results.

REFERENCES

Abramopoulos, F., C. Rosenzweig, and B. Choudhury, 1988: Improved ground hydrology calculations for global climate models (GCMs): Soil water movement and evapotranspiration. *J. Climate,* **1,** 921–941.

Band, L. E., 1993: Effect of land surface representation on forest water and carbon budgets. *J. Hydrol.,* **150,** 749–772.

Bascompte, J., and R. V. Sole, Eds., 1998: *Modeling Spatio-Temporal Dynamics in Ecology*. Springer-Verlag, 210 pp.

Bélair, S., L.-P. Crevier, J. Mailhot, B. Bilodeau, and Y. Delage, 2003: Operational implementation of the ISBA land surface scheme in the Canadian regional weather forecast model. Part I: Warm season results. *J. Hydrometeor.,* **4,** 352–370.

Bonan, G. B., 1993: Importance of leaf area index and forest type when estimating photosynthesis in boreal forests. *Remote Sens. Environ.,* **43,** 303–314.

Campbell, G. S., and J. M. Norman, 1998: *An Introduction to Environmental Biophysics.* Springer-Verlag, 285 pp.

Chen, J. M., 1999: Spatial scaling of a remote sensed surface parameter by contexture. *Remote Sens. Environ.,* **69,** 30–42.

——, J. Liu, J. Cihlar, and M. L. Guolden, 1999: Daily canopy photosynthesis model through temporal and spatial scaling for remote sensing applications. *Ecol. Modell.,* **124,** 99–119.

——, and Coauthors, 2002: Validation of Canada-wide leaf area index maps using ground measurements and high and moderate resolution satellite imagery. *Remote Sens. Environ.,* **80,** 165–184.

——, and Coauthors, 2003: Spatial distribution of carbon sources and sinks in Canada's forests. *Tellus,* **55B,** 622–641.

Chen, W., J. Chen, and J. Cihlar, 2000: An integrated terrestrial ecosystem C-budget model based on changes in disturbance, climate, and atmospheric chemistry. *Ecol. Modell.,* **135,** 55–79.

Chouinard, C., J. Mailhot, H. L. Mitchell, A. Staniforth, and R. Hogue, 1994: The Canadian regional data assimilation system: Operational and research applications. *Mon. Wea. Rev.,* **122,** 1306–1325.

Cihlar, J., J. Chen, and Z. Li, 1997: Seasonal AVHRR multichannel data sets and products for studies of surface-atmosphere interactions. *J. Geophys. Res.,* **102,** 29 625–29 640.

——, J. Beaubien, R. Latifovic, and G. Simard, 1999: Land cover of Canada 1995 version 1.1. Digital data set documentation, Natural Resources Canada. [Available online at ftp://ftp2.ccrs.nrcan.gc.ca/ftp/ad/EMS/landcover95/.]

Côté, J., M. Roch, A. Staniforth, and L. Fillion, 1993: A variable-resolution semi-Lagrangian finite-element global model of the shallow-water equations. *Mon. Wea. Rev.,* **121,** 231–243.

——, S. Gravel, A. Methot, A. Patoine, M. Roch, and A. Staniforth, 1998a: The operational CMC–MRB global environmental multiscale (GEM) model. Part I: Design considerations and formulation. *Mon. Wea. Rev.,* **126,** 1373–1395.

——, J.-G. Desmarais, S. Gravel, A. Methot, A. Patoine, M. Roch, and A. Staniforth, 1998b: The operational CMC–MRB global environmental multiscale (GEM) model. Part II: Results. *Mon. Wea. Rev.,* **126,** 1397–1418.

Dickinson, R. E., A. Henderson-Sellers, P. J. Kennedy, and M. E. Wilson, 1986: Biosphere-Atmosphere Transfer Scheme (BATS) for the NCAR Community Climate Model. National Center for Atmospheric Research Tech. Note NCAR/TN-275 + STR, 169 pp.

——, ——, ——, and F. Giorgi, 1992: Biosphere–Atmosphere Transfer Scheme (BATS) Version 1e as coupled to the NCAR Community Climate Model. National Center for Atmospheric Research Tech. Note., 238 pp.

Ehleringer, J. R., and C. B. Field, Eds., 1993: *Scaling Physiological Processes: Leaf to Globe.* Academic Press, 388 pp.

Entekhabi, D., and P. S. Eagleson, 1989: Land surface hydrology parameterization for atmospheric general circulation models including subgrid scale spatial variability. *J. Climate,* **2,** 816–831.

Garratt, J. R., 1993: Sensitivity of climate simulations to land-surface and atmospheric boundary-layer treatments—A review. *J. Climate,* **6,** 419–449.

Harte, J., A. Kinzig, and J. Green, 1999: Self-similarity in the distribution and abundance of species. *Science,* **284,** 334–336.

Hu, Z., and S. Islam, 1997: A framework for analyzing and designing scale invariant remote sensing algorithm. *IEEE Trans. Geosci. Remote Sens.,* **35,** 747–755.

Jarvis, P. G., 1995: Scaling processes and problems. *Plant Cell Environ.,* **18,** 1079–1089.

Ju, W., and J. Chen, 2005: Distribution of soil carbon stocks in Canada's forests and wetlands simulated based on drainage class, topography and remotely sensed vegetation parameters. *Hydrol. Processes,* **19,** 77–94.

Katul, G., C.-T. Lai, K. Shafer, B. Vidakovik, J. Alberson, D. Ellsworth, and R. Oren, 2001: Multiscale analysis of vegetation surface fluxes: From seconds to years. *Adv. Water Resour.,* **22,** 1119–1132.

Kimball, J. S., S. W. Running, and S. S. Saatchi, 1999: Sensitivity of boreal forest regional water flux and net primary production simulations to sub-grid-scale land cover complexity. *J. Geophys. Res.,* **104,** 27 789–27 802.

Kite, G. W., and A. Pietroniro, 1996: Remote sensing application in hydrological modeling. *Hydrol. Sci.,* **41,** 563–591.

Klita, D. L., and Coauthors, 1998: A comparison between two satellite-based land cover classification programs for a boreal forest region in northwest Alberta, Canada. *Proc. 20th Canadian Symp. on Remote Sensing,* Calgary, AB, Canada, Canada Centre for Remote Sensing and ERIM International Inc., 197–202.

Kucharik, C. J., and Coauthors, 2000: Testing the performance of a Dynamic Global Ecosystem Model: Water balance, carbon balance, and vegetation structure. *Global Biogeochem. Cycles,* **14,** 795–826.

Lacelle, B., 1998: Canada's soil organic carbon database. *Soil Processes and the Carbon Cycle,* R. Lal, J. Kimbla, R. F. Follett, and B. A. Stewart, Eds., CRC Press, 81–92.

Liu, J., J. Chen, J. Cihlar, and W. Chen, 2003: Mapping evapotranspiration based on remote sensing: An application to Canada's landmass. *Water Resour. Res.,* **39,** 1189, doi:10.1029/2002WR001680.

Milne, B. T., and W. B. Cohen, 1999: Multiscale assessment of binary and continuous land cover variables for MODIS validation, mapping and modeling applications. *Remote Sens. Environ.,* **70,** 82–98.

——, V. K. Gupta, and C. Restrepo, 2002: A scale invariant coupling of plants, water, energy and terrain. *EcoScience,* **9,** 191–199.

Oleson, K. W., and G. B. Bonan, 2000: The effects of remotely sensed plant functional type and leaf area index on simulations of boreal forest surface fluxes by the NCAR land surface model. *J. Hydrometeor.,* **1,** 431–446.

Pierce, L. L., and S. W. Running, 1995: The effects of aggregating sub-grid land surface variation on large-scale estimates of net primary production. *Landscape Ecol.,* **10,** 239–253.

Pietroniro, A., and E. D. Soulis, 1999: Assessment of global land-cover data for atmospheric and hydrologic model applications in the Mackenzie basin, Canada. *Proc. Fifth Scientific Workshop for the Mackenzie GEWEX Study,* Edmonton, AB, Canada, Canada Centre for Remote Sensing, 129–133.

Pitman, A. J., 2003: Land surface schemes in climate models. *Int. J. Climatol.,* **23,** 479–510.

Pleim, J. E., and A. Xiu, 2003: Development of a land surface model. Part II: Data assimilation. *J. Appl. Meteor.,* **42,** 1811–1822.

Poveda, G., and S. F. Luis, 2004: Annual and interannual (ENSO) variability of spatial scaling properties of a vegetation index (NDVI) in Amazonia. *Remote Sens. Environ.,* **93,** 391–401.

Rango, A., and A. I. Shalaby, 1999: Urgent operational applications of remote sensing in hydrology. World Meteorological Organization, Operational Hydrology Rep. 43, Secretariat of World Meteorological Organization, Geneva, Switzerland, 211 pp.

Rastetter, E. B., A. W. King, B. J. Cosby, G. M. Hornberger, R. V. O'Neill, and J. E. Hobbie, 1992: Aggregating fine-scale ecological knowledge to model coarser-scale attributes of ecosystems. *Ecol. Appl.,* **2,** 55–70.

Rawls, W. J., L. R. Ahuja, and D. L. Brakensiek, 1992: Estimating soil hydraulic properties from soils data. *Indirect Methods for Estimating Hydraulic Properties of Unsaturated Soils,* M. Van Genuchthen, F. J. Leij, and L. J. Lund, Eds., University of California Riverside Press, 329–341.

Roulet, N. T., P. M. Crill, N. T. Comer, A. Dove, and R. A. Boubonniere, 1997: CO_2 and CH_4 flux between a boreal beaver pond and the atmosphere. *J. Geophys. Res.,* **102,** 29 313–29 320.

Saunders, I. R., J. D. Bowers, Z. Huo, W. G. Bailey, and D. Verseghy, 1999: Simulation of alpine tundera surface microclimates using the Canadian land surface scheme. II. Energy balance and surface microclimatology. *Int. J. Climatol.,* **19,** 1131–1143.

Schut, P., J. Shields, C. Tarnocai, D. Coote, and I. Marshall, 1994: Soil landscapes of Canada—An environmental reporting tool. *Proc. Canadian Conf. on GIS,* Ottawa, ON, Canada, Agriculture Canada, 953–965.

Sellers, P. J., Y. Mintz, Y. C. Sud, and A. Dalcher, 1986: A Simple Biosphere model (SiB) for use within general circulation models. *J. Atmos. Sci.,* **43,** 505–531.

——, M. D. Heiser, and F. G. Hall, 1992: Relationship between surface conductance and spectral vegetation indices at intermediate (100 m2 to 15 km2) length scales. *J. Geophys. Res.,* **97,** 19 033–19 060.

——, and Coauthors, 1995: Effects of spatial variability in topography, vegetation cover and soil moisture on area-averaged surface fluxes: A case study using the FIFE 1989 data. *J. Geophys. Res.,* **100,** 25 607–25 629.

——, and Coauthors, 1996: A revised land surface parameterization (SiB2) for atmospheric GCMs. Part I: Model formulation. *J. Climate,* **9,** 676–705.

——, and Coauthors, 1997a: Modeling the exchange of energy, water, and carbon between continentals and the atmosphere. *Science,* **275,** 502–509.

——, and Coauthors, 1997b: BOREAS in 1997: Experiment overview, scientific results, and future directions. *J. Geophys. Res.,* **102,** 28 731–28 769.

Shields, J. A., C. Tarnocai, K. W. G. Valentine, and K. B. MacDonald, 1991: Soil landscapes of Canada. Procedures manual and user's hand book, Agriculture Canada Publication 1868/E, Ottawa, ON, Canada, 74 pp.

Simic, A., J. Chen, J. Liu, and F. Csillag, 2004: Spatial scaling of net primary productivity using subpixel information. *Remote Sens. Environ.,* **93,** 246–258.

Tarnocai, C., 1996: The amount of organic carbon in various soil orders and ecological provinces in Canada. *Soil Processes and the Carbon Cycle,* R. Lal, J. Kimbla, R. F. Follett, and B. A. Stewart, Eds., CRC Press, 81–92.

Tilman, D., and P. Kareiva, Eds., 1997: *Spatial Ecology*. Princeton University Press, 368 pp.

Turner, D. P., R. Dodson, and D. Marks, 1996: Comparison of alternative spatial resolution in the application of a spatially distributed biochemical model over complex terrain. *Ecol. Modell.,* **90,** 53–67.

Verseghy, D. L., 1991: CLASS: A Canadian land surface scheme for GCMs: I. Soil model. *Int. J. Climatol.,* **11,** 111–133.

——, N. A. McFarlane, and M. Lazare, 1993: CLASS: A Canadian land surface scheme for GCMs: II. Vegetation model and coupled runs. *Int. J. Climatol.,* **13,** 347–370.

Wood, E. F., and V. Lakshmi, 1993: Scaling water and energy fluxes in climate systems: Three land–atmospheric modeling experiments. *J. Climate,* **6,** 839–857.